Nerolidol production in agroinfiltrated tobacco: impact of protein stability and membrane targeting of strawberry (*Fragraria ananassa*) NEROLIDOL SYNTHASE1

Paola Andrade[a,1], David Manzano[a,b], Karla Ramirez-Estrada[a,b], Daniel Caudepon[a,b], Montserrat Arro[a,b], Albert Ferrer[a,b], Michael A. Phillips[c,d*]

[a] Plant Metabolism and Metabolic Engineering Program, Center for Research in Agricultural Genomics, (CRAG) (CSIC-IRTA-UAB-UB), Campus UAB, Bellaterra (Cerdanyola del Vallès), Barcelona, Spain

[b] Department of Biochemistry and Physiology, Faculty of Pharmacy and Food Sciences, University of Barcelona, Barcelona, Spain

[c] Department of Biology, University of Toronto – Mississauga, Mississauga, Ontario, L5L 1C6 Canada

[d] Department of Cellular and Systems Biology, University of Toronto, Toronto, Ontario M5S 3G5, Canada

Author email address: paoandrade1@gmail.com, david.manzano.alias@gmail.com, danielcaugim@gmail.com, montsearroplans@ub.edu, albertferrer@ub.edu, michaelandrew.phillips@utoronto.ca

* To whom correspondence should be addressed: Michael A. Phillips michaelandrew.phillips@utoronto.ca

[1] Present address: Laboratorio de Biotecnología, Instituto de Investigaciones Agropecuarias CRI-La Platina, 8831314 Chile

Abstract (227 words)

The sesquiterpene alcohol nerolidol, synthesized from farnesyl diphosphate (FDP), mediates plant-insect interactions across multiple trophic levels with major implications for pest management in agriculture. We compared nerolidol engineering strategies in tobacco using agroinfiltration to transiently express strawberry (*Fragraria ananassa)* linalool/nerolidol synthase (FaNES1) either at the endoplasmic reticulum (ER) or in the cytosol as a soluble protein. Using solid phase microextraction and gas chromatography – mass spectrometry (SPME-GCMS), we have determined that FaNES1 directed to the ER via fusion to the transmembrane domain of squalene synthase or hydroxymethylglutaryl - CoA reductase displayed significant improvements in terms of transcript levels, protein accumulation, and volatile production when compared to its cytosolic form. However, the highest levels of nerolidol production were observed when FaNES1 was fused to GFP and expressed in the cytosol. This SPME-GCMS method afforded a limit of detection and quantification of 1.54 and 5.13 pg, respectively. Nerolidol production levels, which ranged from 0.5-3.0 μg/g F.W., correlated more strongly to the accumulation of recombinant protein than transcript level, the former being highest in FaNES-GFP transfected plants. These results indicate that while the ER may represent an enriched source of FDP that can be exploited in metabolic engineering, protein accumulation is a better predictor of sesquiterpene production.

Keywords: Terpenes; agroinfiltration, *Nicotiana benthamiana*; volatile analysis; GCMS; solid phase microextraction

1. Introduction

Many plants release volatile organic compounds (VOCs), a subset of natural products with low molecular weights, high vapor pressures, and generally lipophilic properties. A variety of plant biosynthetic pathways yields VOCs, including phenylpropanoids/benzenoids, acyl lipids, and amino acid derivatives [1]. However, the terpenoids (alternatively isoprenoids) compose the largest group both in terms of structural diversity and global annual production in nature [2].

All terpenoids are derived from the polymerization of two branched-chain C_5 olefinic precursors, isopentenyl diphosphate (IDP) and its isomer dimethylallyl diphosphate (DMADP) [3], and play essential roles in the primary metabolism of plants as membrane anchors of various redox cofactors (ubiquinone, plastoquinone, and tocopherol), photosynthetic pigments (carotenoids and chlorophyll side chains), growth regulators (cytokinins, brassinosteroids, gibberellins, strigolactones, and abscisic acid), and membrane stabilizers (phytosterols) [4]. IDP and DMADP are biosynthesized by two independent, compartmentally separated pathways in plant cells: the mevalonate (MVA) pathway [5] and the 2-*C*-methyl-D-erythritol 4-phosphate (MEP) pathway [6]. In general, the plastid localized MEP pathway supplies precursors for the synthesis of monoterpenes (C_{10}), diterpenes (C_{20}), and carotenoids (C_{40}) whereas sesquiterpenes (C_{15}) and the nortriterpene brassinosteroids and sterols ($C_{27\text{-}29}$) are derived from IDP and DMADP synthesized through the MVA pathway, steps of which are localized to the cytosol, the endoplasmic reticulum (ER), and possibly the peroxisome. Detailed genetic [7, 8] and inhibitor studies [9, 10] have confirmed that exchange of common intermediates is limited under most circumstances. However, examples of sesquiterpenes made by MEP pathway precursors and monoterpenes made by MVA precursors have also been reported [11-13], indicating that some sharing of the universal intermediates does take place, usually in specialized tissues and in the context of secondary metabolism.

Most terpenoids may be considered secondary (or specialized) metabolites with functional roles as allelochemicals. Volatile terpenoids (usually olefins with fewer than 20

Abbreviations: FDP, farnesyl diphosphate; GCMS, gas chromatography – mass spectrometry; SPME, solid phrase microextraction; IDP, isopentenyl diphosphate; DMADP, dimethylallyl diphosphate; MEP, 2-*C*-methyl-D-erythritol 4-phosphate; MVA, mevalonate; DMNT, 4,8-dimethyl-1,3,7-nonatriene; FaNES1, *Fragraria x ananassa* linalool/nerolidol synthase; FPS, farnesyl diphosphate synthase; HMGR, 3-hydroxy-3-methylglutaryl-coenzyme A reductase; SQS, squalene synthase

carbons) aid plants by attracting pollinators and seed dispersers [14], mimicking alarm pheromones to disperse insect herbivores [15], or by attracting predatory insects which indirectly aid the plant [16-19]. Nerolidol has shown particular promise in pest management strategies due to its ability to summon herbivore predators when released by host plants under attack [20, 21].

Metabolic engineering strategies have therefore focused on the production of terpenoid volatiles across species to transfer the defensive properties conferred by these compounds. Ectopic expression of strawberry (*Fragraria x ananassa)* linalool/nerolidol synthase (FaNES1) in mitochondria overcame previous side reactions associated with its expression in the cytosol [22] and improved the production of its biologically active breakdown product dimethylnonatriene (DMNT), an approach which succeeded in making Arabidopsis attractive to spider mite predators [23]. It further demonstrated that mitochondria of plants contain appreciable quantities of farnesyl diphosphate (FDP), the precursor to essentially all sesquiterpenes. Moreover, it underscored the importance of compartmentation and FDP availability in sesquiterpene metabolic engineering strategies. Indeed, selective targeting of a geraniol synthase gene in infiltrated *Nicotiana benthamiana* leaves has been employed to compare the availability of geranyl diphosphate (GDP), the precursor to monoterpenes, in various subcompartments of the plant cell [24]. FaNES1 has been used to similar effect to compare tissue specific expression of a terpene synthase in *N. benthamiana* under the control of various promoters by monitoring linalool emissions as well as the accumulation of non-volatile linalool conjugates [25].

Nerolidol is synthesized directly from FDP, a central metabolic intermediate supplied by FDP synthase (FPS). The Arabidopsis genome encodes two *FPS* genes (*FPS1* and *FPS2*) [26]; the dual targeting *FPS1* can produce a protein targeted to the cytosol (FPS1S) or mitochondria (FPS1L) [27] and supplies FDP needed for essential functions through most of the plant life cycle. In contrast, *FPS2* expression is highest in seeds and in developing embryos [28]. While FPS isoforms are soluble, several important enzymes of cytosolic terpenoid metabolism, including 3-hydroxy3-methylglutaryl-coenzyme A reductase (HMGR) and squalene synthase (SQS), are localized to the ER membrane, leading us to hypothesize that this microenvironment may be suitable for sesquiterpene engineering. Previous studies have confirmed that the physiological requirements for FDP must be taken into consideration for engineering strategies as any strong deviations from physiological conditions may result in major developmental

perturbations. For example, while FDP is needed for sterol and ubiquinone biosynthesis in the cytosol and mitochondria, respectively, overexpression of *FPS1L* [29] and *FPS1S* [30] both cause necrotic lesions associated with oxidative stress and depletions in upstream DMADP needed for cytokinin biosynthesis. Co-expression of *FPS1L* and *FaNES1* in mitochondria mitigates these effects [31] . Thus, sesquiterpene engineering in plants is complicated by the dependency of multiple developmental processes, the cellular redox state, and hormone biosynthetic pathways on the steady state concentration of FDP.

Here we describe an alternative strategy to redirect FDP towards sesquiterpene biosynthesis by sesquiterpene synthase targeting to the ER. To test our hypothesis that the ER membrane may foster a microenvironment enriched in FDP which might be exploited to improve sesquiterpene production in plant hosts, we conducted agroinfiltration-transient expression assays in tobacco to evaluate the comparative benefits of the ER membrane versus the cytosol as a subcellular target for recombinant FaNES1 expression. Localization to the ER membrane improved nerolidol production overall compared to expression in soluble form, but the highest levels were seen when FaNES1 was fused to a solubility partner such as GFP. The implications for engineering sesquiterpene biosynthesis in related plants systems are discussed.

2. Methods and materials

2.1 Plant material

N. benthamiana plants were grown in the greenhouse under a 14 h photoperiod with a daytime temperature of 25-27^0 C (22^0 C at night) and 80 μmol photons·m^2·s^{-1} for 6-8 weeks. All plants were grown in potting mixtures consisting of equal parts of perlite, vermiculite and Shrub & Tree mixture #2 (Klasmann Deilmann, Geeste, Germany) and irrigated with Hoagland's solution supplemented with chelated iron (Kelamix, 35 mg·L^{-1}) and micronutrients (B, Cu, Mn, Fe, Mo, and Zn at 0.4 g·L^{-1}).

2.2 Bacterial strains

Agrobacterium tumefaciens strain EHA105 was used in transient expression assays and maintained on YEB media containing rifampicin (150 μg·mL^{-1}) and gentamycin (50 μg·mL^{-1}). For the preparation of transformation vectors, *Escherichia coli* One Shot® TOP10 (Invitrogen, Inc.) were used for bacterial transformations and for the preparation of plasmid stocks.

2.3 Construction of transformation vectors

To direct FaNES1 to the ER membrane in plant cells, the cDNA for FaNES1 was cloned in frame to the sequence encoding the ER transmembrane domains of either 3-hydroxy-3-methylglutaryl-coenzyme A reductase 1S (dmHMGR1S) or squalene synthase (dmSQS). In the first case, a version of *FaNES1* (AX528996) was first amplified by PCR without a stop codon from a pCAMBIA3300-CoxIV-FaNES1 plasmid template using the FaNES1-For-SalI and FaNES1-Rev-SalI primers (see table S1). The 1557 bp product bearing a *Sal*I site at each end was cloned into the pGEM-T Easy vector (Promega). In parallel, the dmHMGR1S transmembrane domain to be fused at the N-terminus of FaNES1 was first cloned by amplifying the region corresponding to amino acids 1 to 178 of *Arabidopsis thaliana* HMGR1S using primers HMGR1S-For-KpnI and HMGR1S-dm-Rev-SalI (see table S1). The 546 bp product was also cloned into pGEM-T Easy and purified in sufficient quantity for a *Kpn*I-*Sal*I digestion and gel purification. This product was subcloned into a pBluescript-SK$^+$ vector (pBS) digested with the same enzymes. A triple repeat of the HA epitope (3HA) obtained from the pE2n vector [32] (GenBank EU334817) was inserted downstream of dmHMGR1S following *SalI-BamHI*

digestion of each and ligation with T4 DNA ligase (Roche) to produce pBS-dmHMGR1S-3HA. This plasmid and the pGEM-T plasmid containing FaNES1-*SalI* were separately digested with *SalI*, purified, and ligated to give pBS-dmHMGR1S-FaNES1-3HA. To compare the effect of ER membrane targeting to the expression of a soluble form of the same enzyme, this entire cloning sequence was repeated except FaNES1 was amplified with primers FaNES1-For-KpnI and FaNES1-Rev-SalI for direct *KpnI*-*SalI* digestion and cloning into pBS without dmHMGR1S, affording pBS-FaNES1-3HA. A similar procedure was used to generate the plasmid pBS-3HA-dmSQS1. The plant transformation vectors were generated by transferring the dmHMGR1S-FaNES1-3HA, 3HA-FaNES1-dmSQS1, and FaNES1-3HA constructs to the pENTR3C donor plasmid via an additional subcloning step. pBS-dmHMGR1S-FaNES1-3HA and pBS-FaNES1-3HA were digested with *SpeI* and blunted with Klenow fragment 3'-5' exonuclease activity according to manufacturer's instructions (Roche). The blunted fragments were then digested with *KpnI* and purified. The mixed sticky end-blunt fragments were subsequently ligated into *KpnI* and *EcoRV* digested pENTR3C. Once dmHMGR1S-FaNES1-3HA, 3HA-FaNES1-dmSQS1, and FaNES1-3HA had been transferred to a Gateway (Invitrogen) entry clone, they were transferred to the pMDC85 (dmHMGR1S-FaNES1-3HA and FaNES1-3HA) or pMDC45 (3HA-FaNES1-dmSQS1) destination vector with LR Clonase II recombinase reactions according the manufacturer's protocols. These vectors add a GFP fusion to the C-terminal of the peptide and is driven by the 35S promoter. All expression vectors were fully sequenced to confirm maintenance of the reading frame.

2.4 Transitory expression in N. benthamiana leaves

The transitory expression of FaNES1 in 4-5 week old *N. benthamiana* was accomplished by syringe infiltration with *A. tumefaciens* strain EHA105. Competent bacteria were heat shock transformed with one of several plasmids for FaNES1 expression (dmHMGR1S-FaNES1-3HA-GFP, GFP-3HA-FaNES1-dmSQS1 or FaNES1-3HA-GFP), ER localization [DSRedT3 in the pMDC83 vector [33] modified for ER targeting and retention [34]], or helper component proteinase (HCPro in the pTRANS5-TEV vector). Transformed cells were plated on solid YEB media containing rifampicin (150 $\mu g \cdot mL^{-1}$) and kanamycin (25 $\mu g \cdot mL^{-1}$). Resistant colonies were tested by PCR to confirm the presence of the expected construct. Positives were grown overnight on a shaker (180 rpm) at 28^0 C in a 3 mL YEB liquid culture with the same antibiotics. A 30 μL aliquot was used to inoculate a 30 mL YEB-rifampicin-

kanamycin culture which was grown overnight under the same conditions. Cultures were diluted to OD_{595} 1.0, and 30 mL were transferred to a 50 mL conical tube. The cells were centrifuged 10 minutes at 3500 rpm using a J20 rotor, and the supernatant was discarded. Pellets were resuspended in 2 mL infiltration buffer consisting of 10 mM $MgCl_2$, 10 mM HEPES, and acetosyringone at either 100 μM (for nerolidol production) or 200 μM (for subcellular localization). The solutions were adjusted to pH 5.6.

For transient nerolidol production, a FaNES1 expression culture listed above was mixed in a 1:1 (*v/v*) ratio with the HCPro expression culture prior to infiltration. For subcellular localization studies, a FaNES1 expression culture was mixed in a ratio of 1:1:1 (*v/v/v*) with the HCPro culture and the ER targeting control vector (DSRedT3).

Syringe infiltration was accomplished by injection of 1 mL culture to the abaxial leaf surface using a 1 mL needleless plastic syringe. Infiltration sites were marked with a permanent marker and plants were subsequently returned to the greenhouse. For subcellular localization, infiltrated plants (n = 3) were observed 0, 2, 3, or 4 days post-infiltration (dpi), whereas plants used for nerolidol production were sampled 0, 2, 3, 4, 6, 9, or 12 dpi.

2.5 RNA extraction, cDNA synthesis, and quantitative PCR

Total RNA was obtained from 100 mg fresh frozen ground tobacco leaf tissue using the PureLink® MiniKit (Ambion, Life Technologies). This was further treated with DNA-free®, DNAse Treatment and Removal kit (Ambion) to remove traces of genomic DNA and quantified using a NanoDrop 2000 (Thermo Fisher Scientific). RNA intengrity was checked using a 1% denaturing agarose gel and 0.5-1.0 μg total RNA for each sample. cDNA was synthesized from 3 μg total RNA using the Superscript® III Reverse Transcriptase (Invitrogen) and poly dT_{18} primer according to manufacturer's instruction and finally diluted 1:40 with water prior to use. This template was amplified in 20 μL quantitative PCR (QPCR) assays, which included 2 μL diluted cDNA, 0.6 μL each forward and reverse primers, 10 μL 2X SYBR Green mix (Roche Diagnostics), and 6.8 μL water. QPCRs were performed on a Roche Lightcycler 480 programmed for a 3 min denaturation step at 94 ^{0}C and 40 cycles of 30 seconds denaturation at 94 ^{0}C and 30 seconds hybridization and extension at 60 ^{0}C. All biological replicates were analyzed in three technical replicates. FaNES1 transcript concentration was quantified on an absolute scale in infiltrated *N. benthamiana* tissue using a 14-point standard curve obtained from

three independently prepared serial dilutions of a the dmSQS-FaNES1-3HA plasmid which bears a single copy of FaNES1. FaNES1 copy number per μg total RNA was calculated based on linear regression of crossing time (C_t) values to the log of amplicon copies (r^2 =0.99). C_t values were obtained using a FaNES1 qPCR For and Rev primers (table S1), and cDNA loading was normalized to the protein phosphatase 2A (PP2A) gene [35] using primers PP2A Nb qPCR For and PP2A Nb qPCR Rev (table S1). Primer efficiencies were determined as described in Pfaffl [36], and the FaNES1 and PP2A primers were found to consistently display efficiencies of 1.91 and 1.93, respectively.

2.6 Protein extraction from N. benthamiana leaves, concentration, and Western blotting

To obtain total protein extracts from infiltrated tobacco leaf tissue, 40 mg of fresh frozen tissue ground in liquid nitrogen was transferred to a 1.5 mL Eppendorf tube. A 200 μL aliquot of protein extraction buffer was added (120 mM Tris-HCl pH 8.6, 40 μM β-mercaptoethanol, 60 μM sodium dodecylsulfate (SDS), 1 mM phenylmethane sulfonylflouride (PMSF), 15 $\mu g \cdot mL^{-1}$ aprotinin, 1.5 $\mu g \cdot mL^{-1}$ E64, 1.5 $\mu g \cdot mL^{-1}$ pepstatin A), mixed by vigorous vortexing until homogenized, and heated to 100 ^{0}C for 10 minutes. This was then centrifuged at 16,000 g for 15 at 4 ^{0}C and the pellet discarded. Concentrations were determined using the Bradford reagent (BioRad) and a calibration curve constructed from bovine serum albumin. SDS-PAGE analysis was carried out using 9% acrylamide gels in a Biorad Protean 3 electrophoresis system according to manufacturer's instructions. A 30 mg aliquot of each protein sample in approximately 20 μL was prepared to which 1/10 vol loading buffer (50% *v/v* glycerol and 1% *w/v* bromphenol blue) was added. Samples were heated at 100 ^{0}C for 5 min before loading. Electrophoresis was carried out at 125 mA for approximately 3 h. Electrotransfer to Hybond-P polyvinylidene difluoride (PVDF) membranes (Amersham Biosciences) was accomplished using a BioRad cassette according to previously published conditions [37]. The membrane was blocked in phosphate buffered saline Tris pH 7.5 (PBS-T) containing 5% (w/v) Blotto non-fat dry milk (Santa Cruz Biotechnology, Inc.) for 16 h at 4°C following a pre-incubation with PBS-T buffer alone for 3 min. Membranes were washed twice for 2 min and twice for 10 min in PBS-T alone, then incubated with the 1:500 diluted primary antibody solution (anti-HA (Y-11) sc-805; Santa Cruz Biotechnology, Inc.) for 1 h at room temperature and washed 4 times in PBS-T for 5 min at room temperature. Washed membranes were then incubated with a secondary antibody consisting of

anti-rabbit anti-IgG conjugated to horseradish peroxidase (Amersham) diluted 1:50,000 in PBS-T with blocking reagent for 1 h at room temperature and again washed as before. Two final washes of 4 min were carried out at room temperature before subjecting the membranes to chemoluminescence detection using an ECL Advanced Western Blotting Detection Kit (Amersham) and LAS 4000 imaging system (Amersham). Uniform loading of protein samples was confirmed by Coomassie staining of membranes following imaging. Western blot band intensity was quantified with Quantity One (Bio Rad).

For tissue fractionation into membrane and soluble fractions, approximately 3 g of *N. benthamiana* agroinfiltrated leaf tissue were harvested from each of three independent plants, cut in small pieces and quickly mixed with 20 mL of ice-cold lysis buffer (0.3M sucrose, 50 mM 3-(-N-morpholino) propanesulfonic acid (pH 7.5) and 5 mM EDTA), supplemented immediately before use with 0.5% (*w/v*) polyvinylpyrrolidone, 5 mM DTT, 5 mM ascorbic acid and a mixture of protease inhibitors for plant tissue extracts (Sigma-Aldrich). Leaf tissue was homogenized with an Ultra Turrax homogenizer (3× 30 s at medium speed on ice) and the resulting homogenate was filtered through two layers of nylon cloth. PMSF (100 mM stock solution) was added to the filtered homogenate to 1 mM final concentration before centrifugation at 10,000 × g for 15 min at 4^0 C to remove cell debris. The resulting supernatant was recovered and centrifuged again at 10,000×g for 15 min at 4^0 C. The pellet was discarded and the supernatant was centrifuged at 100,000 × g for 60 min at 4^0 C to obtain a pellet (P100; membrane fraction) and a supernatant (S100; soluble fraction). The P100 fraction was then resuspended in 10 ml of fresh resuspension buffer (0.3M sucrose, 5mM sodium phosphate (pH 7.8), 0.1 mM EDTA, 1 mM DTT and 1 mM PMSF) and both the S100 and the washed pellet were centrifuged again at 100,000 × g for 60 min at 4^0C. The resulting P100 and S100 fractions were processed once again as described above to obtain the final P100 and S100 fractions. The P100 pellet was subsequently resuspended in 1 mL of resuspension buffer for immunoblot analysis.

For immunoblot analysis, equivalent amounts of P100 (1 to 3 µg of protein) and S100 fractions (15 to 20 µg of protein) from each *N. benthamiana* leaf sample was fractionated by 10% SDS–PAGE, transferred to a nitrocellulose membrane (Amersham, GE Healthcare) and probed using a rabbit anti-GFP antibody (Invitrogen) at a 1:1000 dilution or HA-probe (Santa Cruz Biotechnology) at a 1:500 dilution. Secondary donkey anti-rabbit IgG conjugated to horseradish peroxidase (HPR) was used at a 1:10,000 dilution for the anti-GFP complex. Mouse IgGk light

chain binding protein conjugated to HPR was used at a 1:5,000 dilution to detect the anti-HA complex. The protein-GFP or -HA antibody complexes were visualized using the Amersham ECL Select Western Blotting Detection Reagent (GE Healthcare) according to the manufacturer's instructions and the ChemiDoc Touch (Bio-Rad) for chemiluminescence detection. The blotted membranes were stained for 10 min with a solution of Coomassie Blue (40% (*v/v*) methanol, 7% (*v/v*) acetic acid, 0.025% (*w/v*) Coomasie blue) and washed several times with destining solution (40% (*v/v*) methanol, 7% (*v/v*) acetic acid).

2.7 Quantification of nerolidol production in transfected N. benthamiana *leaves by solid phase microextraction* (*SPME) – gas chromatography mass spectrometry (GCMS)*

To compare the production of nerolidol in tobacco tissue agroinfiltrated with various FaNES1 constructs, we implemented a static headspace SPME - GCMS quantification method optimized for nerolidol detection in fresh tobacco tissue ground in liquid nitrogen. Tissue mass (25 mg – 500 mg FW), exposure time (15 – 45 min), and exposure temperature (30 – 60^0 C) were varied during optimization to maximize sensitivity within the linear range of detection (figure 6). We observed optimal conditions by exposing the SPME fiber (100 μm polydimethylsiloxane, fused silica/SS 24 Ga; Supelco) to 80 mg fresh frozen tobacco tissue in a 10 mL headspace vial fitted with a polytetrafluoroethylene/silicon septum (Supelco) at 40 ^{0}C for 30 min. The linear detector response was established using authentic nerolidol and geraniol standards (unless otherwise specified, all chemical standards were obtained from Sigma-Aldrich) by exposing the fiber to 10, 50, 100, 500, or 1000 ng nerolidol or geraniol standards under these conditions. Except where otherwise noted, all analyses were conducted in triplicate. Once optimal analytical conditions had been established, 100 ng geraniol was added to each sample or control as an internal standard.

Analysis of adsorbed volatiles was performed on a 7890A GC system (Agilent Technologies) fitted with an HP-5ms column (30 m x 0.25 mm ID, 0.25 μm film thickness, Agilent Technologies) running a constant He flow of 1 mL·min^{-1} and coupled to an Agilent 5975C mass selective detector (MSD). The injection port was fitted with a SPME injection port liner set to splitless injection mode. The initial injection port temperature was 30 ^{0}C. Using a programmable temperature vaporization module, it was rapidly heated to 250 ^{0}C following introduction of the

fiber. Oven conditions consisted of an initial temperature of 35 ^{0}C rising to 60 ^{0}C at 3 ^{0}C·min^{-1}, then 5 ^{0}C·min^{-1} to 100 ^{0}C, 8 ^{0}C·min^{-1} to 170, and 10 ^{0}C·min^{-1} to 200 ^{0}C with a hold time of 5 min. This was followed by a cleaning step of 100 ^{0}C·min^{-1} to 325 ^{0}C with a final hold time of 3.67 min. MS data were simultaneously acquired in scan mode (*m/z* 40-350) and selected ion mode (SIM) at *m/z* 69. Electron impact energy was set to 70 eV. Nerolidol was quantified in SIM by comparison of the integrated peak area detected in infiltrated tissue samples to the external standard curve. The geraniol internal standard recovery was estimated by comparison of its integrated peak area in each sample to the peak area of the same amount of geraniol in a control incubation performed without tobacco tissue.

2.8 *Analysis of non-volatile conjugates of nerolidol by tandem LCMS/MS*

Tissue from each *N. benthamiana* treatment group (FaNES1-GFP, GFP empty vector control, FaNES1-GFP, HMGR-FaNES1, FaNES-SQS, or non-infiltrated *N. benthamiana* controls) was lyophilized to dryness for LCMS/MS analysis. A 10 mg powdered tissue aliquot was extracted in 350 μL methanol with 0.1% (*v/v*) formic acid for 1 hour, centrifuged, and filtered through a 0.2 μm telfon syringe filter into a glass LC vial. LCMS/MS analysis was performed on an Agilent 1290 Series II liquid chromatography system coupled to a Sciex 4500Qtrap tandem mass spectrometer. The LC gradient was as follows: 97% buffer A (0.1% (*v/v*) formic acid in ultrapure water) and 3 % buffer B (0.1% (*v/v*) formic acid in acetonitrile) isocratically for 1 min, then a gradient to 25% B by 30 min. Buffer B was then raised to 75% in a single step for 5 min, following by 10 min at initial conditions to re-equilibrate the column. The flow rate was constant at 0.5 mL·min^{-1} and the analytical column was an Agilent Ecplise XDB 150 mm x 4.6 mm fitted with a guard column of the same material. A Q_1 scan in positive mode was performed to detect the following nerolidol conjugates ($M+H^+$) described by Houshyani, et al. (2013): *m/z* 385.2, 401.2, 457.2, 461.3, 503.3, 605.3, 623.3, 647.3, and 691.3. A dwell time of 25 ms was assigned to each mass. Curtain gas was held at 25 psi, and the electrospray interface was set to +4kV and 500 ^{0}C. Peak intensity was normalized to sample mass. Three biological replicates were analyzed from each treatment group.

2.9 Confocoal microscopy and imaging

The expression of FaNES1-GFP fusion proteins in agroinfiltrated tobacco was visualized by fluorescence microscopy using a Leica DC250 fluorescence dissecting microscope. Subcellular

335 localization of constructs bearing ER membrane targeting signals (and controls) was established
336 by imaging on a Leica SPII confocal microscope. At 2-3 days post-infiltration (dpi), green
337 fluorescence was monitored using a 488 nm laser with a BP 498-563 filter. ER membrane
338 localization was established by detection of the ER-targeted form of the DsRed protein, observed
339 with a 568 nm laser and 569-617 filter. Image processing was done with ImageJ and Photoshop
340 Elements.

341

342

3. Results

3.1 Fusion to the transmembrane domains of SQS or HMGR directs FaNES1 to the ER

We expressed FaNES1 in *N. benthamiana* leaves via agroinfiltration with a vector encoding FaNES1 fused to GFP with or without the transmembrane domain of HMGR1S or SQS1. The subcellular localization of these constructs was determined by confocal microscopy 3d following infiltration. Transitory expression assays with GFP alone (figure 1a) or GFP fused to FaNES1 (figure 1b) demonstrated an unambiguous localization of this protein to the cytosolic compartment. When a chimeric construct containing FaNES1 bearing either the transmembrane domain of HMGR1S at its N terminus (figure 1c) or the transmembrane domain of SQS1 at its C terminus (figure 1d) was used instead, green fluorescence was observed in a reticulate structure presumed to be the ER. This was confirmed by merging this image with the signal for DsRedT3, a marker for the ER membrane, obtained from the same sample. This indicated that FaNES1 successfully embeds into the ER membrane when fused to an ER transmembrane domain either at its N or C terminus. The resulting fluorescence in the cytosolic space when FaNES1 was fused to GFP alone indicated that the soluble form of FaNES1 could easily be distinguished from its membrane bound form using this rapid infiltration assay. Some intense spots of fluorescence were observed which did not co-localize with the nucleus and may be attributed to either saturation of the image or localized precipitation of the protein. However, since the DsRed signal coincided with these spots, the former is more likely.

Localization of FaNES to the ER membrane when fused to the transmembrane domain of HMGR or SQS was further verified by purification of the membrane fractions by ultracentrifugation and Western blot analysis of the resulting soluble and membrane fractions. Western blot analysis showed a clear signal from the recombinant protein in the membrane fraction of HMGR-FaNES or FaNES-SQS infiltrated plants whereas no protein was detected in the soluble fraction of these same samples (figure 2A). When this same analysis was performed on plants infiltrated with FaNES alone or fused to GFP, the opposite pattern was observed: recombinant protein was only detected in the soluble fraction and not in the membrane fraction (figure 2B). These results were consistent with our confocal microscopy data which indicated

that the presence of the transmembrane domain of either HMGR or SQS was sufficient to direct and embed FaNES into the ER membrane.

3.2 Fusion of FaNES1 to transmembrane domains or C-terminal sequences results in higher transcript abundance

Steady state transcript levels of various FaNES1 constructs were compared using an absolute, quantitative real time PCR (qRT-PCR) assay. Because FaNES1 is absent from the tobacco genome, measurement of transcripts was based on an external standard curve using known copy numbers of FaNES1-bearing plasmids in qRT-PCR assays. Based on the linear regression of C_t values and plasmid copy number, we calculated the absolute concentration of FaNES1 transcripts in transfected tobacco tissue. Transcripts were readily quantifiable in all cases (figure 3), with the exception of the empty vector control. This analysis demonstrated an approximately 7-fold difference between the absolute transcript level of FaNES1 alone and dmHMGR1S-FaNES1 (all constructs included a triple HA epitope used for Western blot detection). Two constructs bearing coding sequences at the 3' end of FaNES1 (dmSQS1 or GFP) similarly displayed marked improvements in overall transcript abundance when compared to FaNES1 alone, resulting in an approximately 4-fold increase in FaNES1 transcript abundance. Overall, the presence of additional coding sequence at both the 5' and 3' ends of FaNES1 correlated with improved accumulation of FaNES1 transcripts compared to FaNES1 fused only to 3HA.

3.3 Directing chimeric FaNES1 to the ER leads to greater protein accumulation compared to the soluble form

FaNES1 protein accumulation in leaves transfected with these various constructs was measured by Western blot using an anti-HA primary antibody at 3, 6, 9, or 12 days post-infiltration (dpi). Consistent with our mRNA transcript data, the ER membrane bound forms of FaNES1 were easily detectable at all time points (figure 4A; for full gel images, see supplemental data). In contrast, protein from the FaNES1 only construct was virtually undetectable in these assays despite transcript levels were clearly measurable in plants transfected with the FaNES1-3HA construct. These results suggested that transcripts were of

limited value in predicting protein accumulation levels. Our results may also reflect the improved protein stability conferred by embedding FaNES1 in the ER membrane.

The dmHMGR1S-FaNES1 construct reproducibly displayed higher levels of protein than FaNES1-dmSQS1 at 3 dpi (figure 4A). Protein levels for both constructs tapered off from 6 to 12 days but retained detectable levels of expression through the duration of the assay.

This time course was repeated and monitored 2 and 4 dpi to refine our assessment of the kinetics of protein production from these constructs (figure 4B). High levels of protein expression were seen for both ER anchored forms of FaNES1 as early as 2 dpi, confirming that the highest levels of expression are observed in the initial days following agroinfiltration. This experiment also failed to detect the soluble, cytosolic form of FaNES1 (FaNES1-3HA, while confirming the previous observation that FaNES1 anchored to the ER by way of the HMGR1 domain (HMGR1S-FaNES1) generally displayed higher accumulation levels than FaNES1 anchored to the ER through the SQS1 transmembrane domain.

The lack of detectable FaNES1 expressed as a soluble, cytosolic protein in spite of readily detectable transcript levels may be due to rapid turnover of this peptide. This situation was considerably improved when FaNES1 was expressed as a soluble protein fused to GFP. Surprisingly, protein levels of the FaNES1-GFP fusion (figure 5C) were even higher than either ER-directed chimera (figure 5A-B). This reinforced our prior observation that transcript levels, while serving as a useful indicator, do not necessarily predict overall levels of protein accumulation. In these assays, the stability of the fusion partner appears to play a larger role in the accumulation of recombinant proteins than the absolute abundance of transcripts (figure 5D).

3.4 Quantification of nerolidol and its conjugates in agroinfiltrated N. benthamiana *leaves*

In order to compare the ability of these different constructs to support nerolidol biosynthesis *in planta*, we assayed nerolidol production in agroinfiltrated tobacco tissue using a quantitative SPME-GCMS protocol. We optimized critical variables in this assay to ensure that different levels of nerolidol production in transfected *N. benthamiana* tissue could be accurately compared in a linear fashion. Thus, the optimal exposure time and temperature were evaluated for these assay conditions using a nerolidol standard, and the linear response range of nerolidol was determined using different amounts of transfected tissue (figure 6). Using these optimized parameters, we quantified nerolidol production in different transformed tissue samples using an

external curve generated with an authentic nerolidol standard. Geraniol, which is not produced by FaNES1 or tobacco leaf tissue, was added to assess matrix effects.

Using this approach, we determined the average levels of nerolidol production in each construct. When normalized to fresh tissue weight, we observed the highest level of nerolidol production from the soluble GFP fusion (FaNES1-GFP), followed by the two ER anchored forms (dmHMGR1S-FaNES1 followed by FaNES1-dmSQS1) (figure 7A). In contrast, no nerolidol was detected in non-transfected tissue or in tissue transfected with an empty vector control. Tissue transfected with the FaNES only construct likewise did not produce detectable nerolidol in these assays, consistent with the low levels of protein detected by Western blot (figure 2). Geraniol was added to each SPME fiber incubation as an internal standard. However, because recoveries were low (3-4%), nerolidol levels in figure 7 were not corrected using these values and instead are presented as a direct comparison to the external nerolidol standard. Therefore, the actual level of nerolidol production may be much higher.

When nerolidol production quantified by this SPME-GCMS approach was normalized to protein detected by Western blots (figure 5D), we observed similar levels of nerolidol production from both ER targeted constructs (figure 7B). Although the FaNES1-GFP construct demonstrated a higher average value, this difference, compared to dmHMGR1S-FaNES1 and FaNES1-dmSQS1, was not statistically significant ($p = 0.12$ and 0.08, respectively), indicating that the three different chimeric forms are comparable in terms of catalytic efficiency and access to substrate, both in the cytosolic compartment as well as at the ER membrane.

Leaf tissue from each infiltrated plant was extracted for LCMS/MS analysis to assess the accumulation of non-volatile glycosylated forms of nerolidol. Based on Houshyani, et al. (2013), a variety of previously reported conjugated nerolidol metabolites were surveyed using Q_1 selected ion monitoring, constant neutral loss scanning, and precursor and product scans for the expected metabolites using a triple quadrupole tandem MS/MS system. However, most of the peaks matching the expected masses were also present in empty vector controls though absent in non-infiltrated controls. We identified a series of peaks specific to constructs expressing FaNES1 which also matched the nerolidol conjugates described by Houshyani, et al. One such peak, with a predicted neutral mass of 456.2, corresponded to hydroxylnerolidol-malonyl-ketopentoside (figure 8). We selected this peak for further investigation to infer the comparative accumulation of non-volatile conjugates among the different ER embedded or soluble forms of FaNES1. As

can be seen in figure 8, this peak (24.92 min) was only visible in FaNES1-GFP, HMGR-FaNES1, and FaNES1-SQS). No signal was detected at this position in either non-infiltrated controls, empty vector controls (GFP only), or in FaNES1 only expressing tissue. Average peaks areas in these samples were normalized to sample mass (figure 9). The relative levels of accumulation of this nerolidol conjugate matched the free nerolidol observed by GCMS analysis (figure 7), suggesting that while some conjugation of nerolidol evidently took place, it closely mirrored the production of free nerolidol and did not depend on the construct or subcellular localization.

4. Discussion

4.1 Plant secondary metabolites naturally present in trace quantities underscore the need for metabolic engineering

Augmenting the production of volatile terpenoids in plants has become a major biotechnological imperative in recent years due to their importance in agricultural pest management, as fragrances and flavorings, and as chemical feedstocks for biofuel production and other industrial processes [38]. The yield of terpenoids with pharmaceutical or industrial value from natural sources is often low due to the high energetic cost of producing specialized metabolites and the specialized tissues needed to store or emit them. Currently, the genetic resources for breeding terpenoid production traits in crops and model plants are poorly developed, while chemical synthesis is only profitable for a tiny fraction of potentially beneficial terpenoids [39]. Metabolic engineering in native or heterologous hosts may therefore represent the only feasible approach to achieving economically sustainable yields of these useful plant natural products. Here we have chosen the agroinfiltration protocol using *N. benthamiana* [40] for evaluating the metabolic engineering of the sesquiterpene alcohol nerolidol, a volatile terpenoid involved in indirect plant defenses against herbivores through the attraction of herbivore predators.

4.2 Subcellular localization of FaNES1 at the outer surface of the ER membrane

We chose *N. benthamiana* to explore nerolidol metabolic engineering strategies because of its rapid and simple agroinfiltration transient expression protocol [41] and demonstrated usefulness in terpenoid metabolic engineering [42, 43]. We explored the outer surface of the ER as a potential source of FDP to sustain nerolidol biosynthesis and confirmed that FaNES1 could readily be translocated into the ER membrane by fusion to either the transmembrane domain of SQS (C-terminus) or HMGR (N-terminus) (figure 1). A similar strategy was employed to engineer isoflavone metabolism in tobacco, wherein chalcone isomerase was directed to the ER by fusion to isoflavone synthase (IFS) [44], an approach which resulted in significant increases in genistein and genistein glycoside accumulation compared to plants transformed with IFS alone.

As a bifunctional enzyme, FaNES1 can use both GDP and FDP to produce linalool and nerolidol, respectively, and a plastid directed form has been previously used in *N. benthamiana* agroinfiltration experiments to examine the potential for linalool production in plastids [45]. *N. benthamiana* agroinfiltration with FaNES1 and other terpene synthases has been exploited as a sensitive indicator of the prenyl diphosphate pools present in different subcellular environments [24]. There, Dong et al. used geraniol synthase to show that trafficking of GDP directly from mitochondria to plastids occurred at a significant rate, demonstrating that our understanding of the exchange of prenyl diphosphates between compartments is still in its infancy. The production of oxygenated terpenes in both Arabidopsis and tobacco has been limited by the conjugation of the available alcohol groups to sugars and organic acids, thus necessitating the analysis of non-volatile forms by LCMS/MS to fully evaluate engineering strategies, as discussed below.

Transient expression of FaNES1 in plastids did not evidently result in the production of detectable nerolidol in this system [45], consistent with the generally accepted absence of FDP in this compartment. However, when FaNES1 was targeted to chloroplasts in stably transformed Arabidopsis, transgenic plants produced not only linalool (presumably from GDP) but also small amounts of nerolidol [22], suggesting that small amounts of FDP may be present in plastids of some species or that incomplete translocation or catalysis during transport may also represent competitive processes. Our initial hypothesis that ER targeting of FaNES1 might facilitate nerolidol production was based on the observation that both SQS [46] and HMGR [47] are functionally embedded in the ER membrane, leading us to hypothesize that this microenvironment may represent an enriched source of FDP which could be exploited for sesquiterpene production. FDP is known to be present in at least two compartments in plant cells: the cytosol and mitochondria, each pool presumably supplying a distinct metabolic pathway. Previous work on Arabidopsis FPS indicated that the long form transcript, *FPS1L*, encodes a protein bearing a targeting peptide directing the preprotein to mitochondria, while the shorter version, *FPS1S*, produces a gene product which is directed to the cytosolic compartment [27]. Mitochondrial FDP is thought to supply ubiquinone biosynthesis, while FDP in the cytosol mainly provides substrate for sterol biosynthesis via SQS. Based on our results, we conclude that the ER membrane is a viable site for FDP substrate availability when compared to the cytosol.

4.3 ER targeting of FaNES1 improves nerolidol production over cytosolic expression but fusion to GFP affords the highest yields

The ability of FaNES1 constructs directed to the cytosol or ER to support nerolidol production was assessed at the transcript, protein, and metabolite level. Embedding the recombinant protein in the ER membrane conferred a distinct advantage in terms of transcript levels (figure 2) and protein stability (figures 3 and 4), as noted by the discrepancy between transcript and protein levels for the soluble form of FaNES1 (FaNES-3HA) compared to constructs directing the expression of FaNES1 as a fusion with a transmembrane domain. The reasons for this discrepancy are currently unknown. FaNES1-3HA generated the lowest transcript levels overall (figure 2). The lack of FaNES1 protein accumulation in soluble form, possibly due to rapid turnover of this protein or poor solubility, further reinforced the benefits of directing this enzyme to the ER. These results support our initial hypothesis that targeting FaNES1 to the ER membrane displays clear advantages over expression of this protein in its soluble form, both in terms of transcript accumulation as well as protein stability. Moreover, when nerolidol production was normalized to the amount of protein detected in Western blots (figure 7), the surface of the ER proved to be at least as proficient at supplying FDP to FaNES1 as the cytosolic compartment and, indeed, offered advantages over cytosolic expression in terms of transcript and protein accumulation. These advantages disappeared on the absolute scale of nerolidol production when these ER targeted chimeras were compared to FaNES1 fused to a highly soluble protein like GFP. We observed the highest overall level of nerolidol production from the FaNES1-GFP construct, evidently a consequence of the higher levels of protein expression observed with this construct which in turn may reflect the exceptional solubility of proteins fused to GFP. Thus, while the surface of the ER is an effective site to direct sesquiterpene formation, our results indicate that the level of protein accumulation (and solubility) is the more important factor for maximizing nerolidol production, provided it occurs in a subcellular location with comparable FDP availability. However, it should be noted that fusion to GFP may not enhance the activity of all proteins, and its usefulness must be evaluated on a case by case basis.

4.3 Static headspace SPME-GCMS analysis of nerolidol production in tobacco

This static headspace SPME assay for nerolidol production in agroinfiltrated tobacco permitted us to rapidly and quantitatively screen different metabolic engineering strategies. This procedure was adapted from previously established methods for quantitative volatile analysis, which may involve static or dynamic volatile collection or sampling techniques using intact, detached, or ground plant tissue [48]. For instance, the continuous, low-level emission of floral volatiles may necessitate detached flowers and the use of a volatile collection trap (VCT) to retain volatiles onto an adsorbent matrix through which airflow is continuously passed for a number of hours [49]. The trapped volatiles can then be eluted with an organic solvent for analysis. On the other hand, static headspace sampling with a SPME fiber may be more appropriate for stored volatile oils or those produced in heterologous systems such as agroinfiltrated tobacco or transgenic Arabidopsis [22]. We found SPME sampling of homogenized plant tissue in sealed headspace vials to be the most effective method for quantitative comparison of different transgene constructs due to the uniformity afforded by using a standardized mass of ground tissue in each assay heated to a consistent temperature during absorption assays. Using this approach, the linear range of tissue mass used in incubations could be unambiguously established (figure 6D). Incubation time and temperature were similarly optimized for headspace sampling with fresh frozen ground tobacco tissue. Static headspace SPME sampling has previously been applied to the analysis of nerolidol in beverages, including wine [50], tea [51], and tequila [52], and a similar strategy was also employed to measure nerolidol in fresh puréed strawberry tissue [53]. To our knowledge, this is the first application of a static headspace SPME method to guide nerolidol metabolic engineering strategies.

The principal drawback to this technique is the low recovery of the internal standard geraniol, suggesting that there is a potent matrix effect of the fresh frozen tobacco tissue, which may retain appreciable levels of nerolidol. However, organic extraction of the same tissue did not improve the sensitivity toward nerolidol in our experimental system. Due to the low recovery of the internal standard (typically 3-4% based on analysis of the same quantity of geraniol without frozen tissue present), we chose not to infer the true level of nerolidol based on internal standard recovery. However, the actual amount of nerolidol produced may be much higher than what we have reported here. Nonetheless, the uniformity of internal standard recovery indicated that these matrix effects were consistent across agroinfiltration experiments. For the purpose of rapidly evaluating the efficacy of different subcellular localization strategies, the use of a SPME volatile

collection of agroinfiltrated tobacco tissue remains an effective technique. When a higher yield of internal standard is essential, increased incubation temperatures may provide some improvements. Likewise, alternative SPME polymers not employed here may demonstrate a higher affinity for geraniol. Finally, the use of organic solvents could foreseeably be optimized to improve internal standard recoveries.

We examined nerolidol conjugates by LCMS/MS based on the observation by Aharoni, et al [54], Houshyani et al [31], and other reports [55] that a significant portion of ectopically produced terpenoids remain sequestered as non-volatile storage forms. We observed many of the expected metabolites whose masses match the conjugates described by Houshyani et al in agroinfiltrated tobacco expressing FaNES in various forms, and these peaks were generally absent from non-infiltrated control tissue. However, many of these same signals were indeed present in empty vector infiltration controls, limiting their usefulness for the evaluation of conjugated nerolidol in FaNES1-transfected tissue. These results may stem from isobars arising from endogenous plant defense compounds which cannot be readily distinguished from nerolidol conjugates under the unit mass resolution of the triple quadrupole system used for this analysis. However, we discerned a number of features which correlated only with FaNES1-transfected tissue whose general characteristics matched previously described nerolidol conjugates, including hydroxylnerolidol-malonyl-ketopentoside (nominal mass 456). Using this feature to infer the degree of sequestration of nerolidol as non-volatile conjugates, we determined that the relative levels closely matched the free, volatile nerolidol measured by GCMS in FaNES, FaNES-GFP, HMGR-FaNES, and FaNES-SQS infiltration experiments (figures 7 and 9). From these observations, we conclude that while some trapping of nerolidol does take place with our engineering strategy, it closely mirrors the overall nerolidol production and does not appear to indicate that one subcellular location is more apt to induce conjugation than another.

N. benthamiana has in recent years proven itself to be the most versatile model system for the study of plant metabolic engineering, largely due to the facile nature of transient expression in this species. The results presented here extend our understanding of the subcellular environment at the ER and the availability of FDP in the cytosolic compartment. Indeed, the technique of SPME sampling of agroinfiltrated plant tissue is widely applicable to the study of plant volatile biosynthesis outside the terpenoid domain. Thus, a similar analytical approach can be used to evaluate efforts to engineer green leaf volatiles and other fatty acid derivatives,

benzenoids, apocarotenoids, and volatile phenylpropanoid derivatives. Future efforts will focus on additional classes of plant volatiles produced in agroinfiltrated tobacco in addition to other species.

629

630 Supplemental Table S1

631 Primers used in this study

Primer name	5’ to 3’ sequence
FaNES1-For-SalI	**GTCGAC**ATGAACGTTGAAACCAAGCATAC
FaNES1-Rev-SalI	**GTCGAC**CATTGATACAGTCTCATACAAC
HMGR1S-For-KpnI	**GGTACC**ATGGATCTCCGTCGGAGGCCTC
HMGR1S-dm-Rev-SalI	**GTCGAC**CGATTTCACAATCTCCTCGTCTTC
FaNES1-For-BamHI	**GGATCC**ATGAACGTTGAAACCAAGCATAC
aNES1-Rev-XbaI	**TCTAGA**CATTGATACAGTCTCATACAA
SQS1-dm-For-XbaI	**TCTAGA**AAGACAAAGGTTGACAAGAAC
SQS1-dm-Rev-NotI-SpeI	**GCGGCCGCACTAGT**TCAGTTTGCTCTGAGATAT
FaNES1-For-KpnI	**GGTACC**ATGAACGTTGAAACCAAGC ATAC
FaNES1-Rev-SalI	**GTCGACC**ATTGATACAGTCTCATACAAC
FaNES1 qPCR For	CTTCGACTCTGGGACGATTTAG
FaNES1 qPCR Rev	GAACAGCCTTCATGTTCCTCTA
PP2A Nb qPCR For	GACCCTGATGTTGATGTTCGCT
PP2A Nb qPCR Rev	GAGGGATTTGAAGAGAGATTTC

632

633

633

634 Figure legends

635 Figure 1. Confocal micrographs of tobacco epidermal parenchyma 3 days after agroinfiltration
636 with *Agrobacterium tumefaciens* harboring a binary plasmid for the expression of GFP alone (a),
637 FaNES1 fused to GFP (b), or FaNES1 fused to the transmembrane domain of HMGR1S (c) or
638 SQS (d). The GFP signals of (c) and (d) correspond to a reticulate structure which co-localizes
639 with the signal for DsRedT3, a marker for the ER membrane (merged signals shown at right).
640 The GFP control, in contrast, is dispersed throughout the cell and is typical of soluble expression
641 in the cytosol. Bar = 20 μm (a and b) or 10 μm (c and d).

642

643 Figure 2. Western blot analysis using anti-HA (A) and anti-GFP (B) antibodies of microsomal
644 (P) and soluble (S) cell fractions from leaves expressing the recombinant FaNES1 proteins and
645 GFP. The predicted molecular weight of FaNES1 proteins is approximately 50.0 kDa (FaNES1-
646 3HA), 83.6 kDa (HMGR-FaNES1-3HA), 71.3 kDa (3HA-FaNES1-SQS), 87.3 kDa (FaNES1-
647 GFP). Coomassie Brilliant Blue-stained large subunit of Rubisco in blotted membranes is shown
648 at the bottom. The position of protein molecular-weight standards is shown on the left.
649 Figure 2. Absolute transcript abundance of *FaNES1* detected in agroinfiltrated *N. benthamiana*.
650 cDNA loading was normalized using the Ct value of reference gene *PP2A*, and the corrected
651 signal was compared to a standard curve constructed from serial dilutions of a purified plasmid
652 containing FaNES1. Values shown represent the average of 3 biological replicates (n = 3). Error
653 bars signify the standard deviation.

654

655 Figure 3. Absolute transcript abundance of FaNES1 detected in agroinfiltrated N. benthamiana.
656 cDNA loading was normalized using the Ct value of reference gene PP2A, and the corrected
657 signal was compared to a standard curve constructed from serial dilutions of a purified plasmid
658 containing FaNES1. Values shown represent the average of 3 biological replicates (n = 3). Error
659 bars signify the standard deviation. 3HA indicates three tandem copies of the hemagglutinin
660 epitope used for Western blot detection. p values for a two tailed t-test are displayed for the
661 corresponding comparison to FaNES1-3HA.

662

Figure 4. Western blot showing an extended (A) or short term (B) time course of protein accumulation in agroinfiltrated N. benthamiana leaf tissue from 0-12 days post infiltration (dpi). The accumulation of FaNES1 fused to the transmembrane domain of HMGR1S at its N-terminus (dmHMGR1S-FaNES1-3HA), the transmembrane domain of SQS1 at its C-terminus (3HA-FaNES1-dmSQS1), or soluble FaNES (FaNES-3HA) are shown. All proteins contained a triple HA epitope for antibody detection. Uniform protein loading of the gel was verified by Coomassie blue staining of Rubisco large subunit (bottom).

Figure 5. Chemoluminescence imaging of a Western blot showing relative expression levels of three FaNES1 constructs targeted to the ER (A and B) or fused to GFP as a soluble protein (C). Agroinfiltrated tobacco leaves transfected with one of the three constructs shown above were harvested 2 days post infiltration. A 2.5 μg aliquot of total protein was electrophoresed on a 9% SDS-PAGE gel, transferred to a PVDF membrane, and imaged via bioluminescent assay of the resulting Western blot, as described in methods. Three independent replicates are shown for each construct. The FaNES1-GFP fusion showed consistently higher protein accumulation levels. D, chemoluminescent signal intensity of the band corresponding to each transgene product shown in A-C (n = 3, error bars represent the standard error).

Figure 6. Optimization of nerolidol quantification by SPME-GCMS. A, differing amounts of nerolidol were added to a headspace vial to determine the linear range of the detector response. Over the likely range of nerolidol production in tobacco, the response range was linear. B, SPME fiber incubations with nerolidol standard were carried out at different temperatures to determine the optimal binding temperature. C, Exposure times ranging from 15 min – 45 min were assays to assess the optimal incubation time. D, Nerolidol standard was assayed in the presence of variable amounts of fresh ground tobacco tissue ranging from 10 mg – 500 mg to assess matrix effects. Beyond 100 mg tissue, significant matrix effects were evident.

Figure 7. Nerolidol production in agroinfiltrated tobacco leaves normalized to tissue fresh weight (A) or FaNES1 protein accumulation level (B). Three biological replicates were analyzed per group. Values shown are uncorrected but internal standard recoveries were typically 3-4%. Actual nerolidol production may therefore be much higher.

Figure 8. LCMS/MS analysis of methanolic extracts of agroinfiltrated tobacco leaf tissue. Q_1 multiple ion monitoring was performed in positive mode to survey nearly a dozen conjugated forms of nerolidol ranging in mass from *m/z* 456 to 690. Peaks also detected in empty vector infiltration controls were ruled out from this comparison. Three individual tobacco plants were infiltrated with each construct. A single representative chromatogram is shown for each construct. The arrow represents one of several nerolidol conjugates used to infer the accumulation of non-volatile forms of nerolidol which was absent from controls. This peak (24.92) matches the expected mass of hydroxynerolidol-malonyl-ketopentoside (457.2 [$M+H^+$]) (Houshyani et al. 2013).

Figure 9. Relative quantification of a non-volatile nerolidol conjugate in agroinfiltrated tobacco leaves. A peak eluting at approximately 24.92 min representing hydroxynerolidol-malonyl-ketopentoside (Houshyani et al. 2013) was used to compare the accumulation of conjugated nerolidol glycosides. This peak was absent in non-infiltrated and empty vector controls and was used to infer accumulation of conjugated forms of nerolidol. Their accumulation closely mirrors the ratios of free nerolidol detected by GCMS in the same treatment groups. The data shown represent peak area normalized to sample mass. Error bars represent the standard error of 3 independent biological replicates.

Acknowledgements

This work was funded in part by grants from the Spanish Government (AGL2013-43522-R) and the Generalitat de Catalunya (2014SGR-1434) to A. F., and by the CERCA Programme/Generalitat de Catalunya. We also acknowledge financial support from the Spanish Ministry of Economy and Competitiveness through the "Severo Ochoa Programme for Centres of Excellence in R&D" 2016-2019 (SEV-2015- 0533). In addition, this work was also supported by grants from the Natural Sciences and Engineering Research Council of Canada (grant number RGPIN-2017-06400) and by the Canadian Foundation for Innovation (project 36131) (to M.P.). The authors give thanks to Harro Bouwmeester of the University of Amsterdam (Holland) for supplying the linalool/nerolidol synthase1 plasmid. Conflict of interest: none.

References cited

1. Dudareva, N., Klempien, A., Muhlemann, J.K. and Kaplan, I. (2013) Biosynthesis, function and metabolic engineering of plant volatile organic compounds. New Phytologist 198 (1), 16-32.
2. Banerjee, A. and Sharkey, T.D. (2014) Methylerythritol 4-phosphate (MEP) pathway metabolic regulation. Natural Product Reports 31 (8), 1043-1055.
3. Gershenzon, J. and Kreis, W. (1999) Biochemistry of terpenoids: monoterpenes, sesquiterpenes, diterpenes, sterols, cardiac glycosides and steroid saponins. In Annual Plant Reviews: Biochemistry of Plant Secondary Metabolism (Wink, M. ed), pp. 222-299, Sheffield Academic Press.
4. Bouvier, F., Rahier, A. and Camara, B. (2005) Biogenesis, molecular regulation and function of plant isoprenoids. Progress in Lipid Research 44 (6), 357-429.
5. Bach, T.J., Boronat, A., Campos, N., Ferrer, A. and Vollack, K.-U. (1999) Mevalonate biosynthesis in plants. Critical reviews in biochemistry and molecular biology 34 (2), 107-122.
6. Phillips, M.A., León, P., Boronat, A. and Rodríguez-Concepción, M. (2008) The plastidial MEP pathway: unified nomenclature and resources. Trends Plant Sci 13 (12), 619-623.
7. Guevara-García, A., San Román, C., Arroyo, A., Cortés, M.E., Gutiérrez-Nava, M.D. and León, P. (2005) Characterization of the Arabidopsis *clb6* mutant illustrates the importance of post-transcriptional regulation of the methyl-D-erythritol 4-phosphate pathway. Plant Cell 17 (2), 628-643.
8. Gutierrez-Nava, M.D.L., Gillmor, C.S., Jimenez, L.F., Guevara-Garcia, A. and Leon, P. (2004) Chloroplast biogenesis genes act cell and noncell autonomously in early chloroplast development. Plant Physiology 135 (1), 471-482.
9. Rodríguez-Concepción, M., Forés, O., Martínez-García, J.F., González, V., Phillips, M.A., Ferrer, A. and Boronat, A. (2004) Distinct light-mediated pathways regulate the biosynthesis and exchange of isoprenoid precursors during Arabidopsis seedling development. Plant Cell 16 (1), 144-56.
10. Laule, O., Furholz, A., Chang, H.S., Zhu, T., Wang, X., Heifetz, P.B., Gruissem, W. and Lange, B.M. (2003) Crosstalk between cytosolic and plastidial pathways of isoprenoid biosynthesis in *Arabidopsis thaliana*. P Natl Acad Sci USA 100 (11), 6866-6871.
11. Opitz, S., Nes, W.D. and Gershenzon, J. (2014) Both methylerythritol phosphate and mevalonate pathways contribute to biosynthesis of each of the major isoprenoid classes in young cotton seedlings. Phytochemistry 98, 110-119.
12. Dudareva, N., Andersson, S., Orlova, I., Gatto, N., Reichelt, M., Rhodes, D., Boland, W. and Gershenzon, J. (2005) The nonmevalonate pathway supports both monoterpene and sesquiterpene formation in snapdragon flowers. P Natl Acad Sci USA 102 (3), 933-938.
13. Wölwer-Rieck, U., May, B., Lankes, C. and Wüst, M. (2014) Methylerythritol and mevalonate pathway contributions to biosynthesis of mono-, sesqui-, and diterpenes in glandular yrichomes and leaves of *Stevia rebaudiana* Bertoni. Journal of Agricultural and Food Chemistry 62 (11), 2428-2435.
14. Gershenzon, J. and Dudareva, N. (2007) The function of terpene natural products in the natural world. Nature Chem Biol 3, 408-414.
15. Crock, J., Wildung, M. and Croteau, R. (1997) Isolation and bacterial expression of a sesquiterpene synthase cDNA clone from peppermint (Mentha x piperita, L.) that produces the

aphid alarm pheromone (E)-β-farnesene. Proceedings of the National Academy of Sciences 94 (24), 12833-12838.
16. Rasmann, S., Kollner, T.G., Degenhardt, J., Hiltpold, I., Toepfer, S., Kuhlmann, U., Gershenzon, J. and Turlings, T.C.J. (2005) Recruitment of entomopathogenic nematodes by insect-damaged maize roots. Nature 434 (7034), 732-737.
17. Turlings, T.C., Tumlinson, J.H. and Lewis, W.J., Exploitation of herbivore-induced plant odors by host-seeking parasitic wasps, Science, 1990, pp. 1251-1253.
18. Boland, W., Feng, Z., Donath, J. and Gäbler, A. (1992) Are acyclic C11 and C16 homoterpenes plant volatiles indicating herbivory? Naturwissenschaften 79 (8), 368-371.
19. Bouwmeester, H.J., Verstappen, F.W.A., Posthumus, M.A. and Dicke, M. (1999) Spider mite-induced (3*S*)-(*E*)-nerolidol synthase activity in cucumber and lima bean. The first dedicated step in acyclic C11-homoterpene biosynthesis. Plant Physiol 121 (1), 173-180.
20. Kos, M., Houshyani, B., Overeem, A.-J., Bouwmeester, H.J., Weldegergis, B.T., van Loon, J.J.A., Dicke, M. and Vet, L.E.M. (2013) Genetic engineering of plant volatile terpenoids: effects on a herbivore, a predator and a parasitoid. Pest Management Science 69 (2), 302-311.
21. Chan, W.-K., Tan, L., Chan, K.-G., Lee, L.-H. and Goh, B.-H. (2016) Nerolidol: A Sesquiterpene Alcohol with Multi-Faceted Pharmacological and Biological Activities. Molecules 21 (5), 529.
22. Aharoni, A., Giri, A.P., Deuerlein, S., Griepink, F., de Kogel, W.-J., Verstappen, F.W.A., Verhoeven, H.A., Jongsma, M.A., Schwab, W. and Bouwmeester, H.J. (2003) Terpenoid metabolism in wild-type and transgenic Arabidopsis plants. Plant Cell 15 (12), 2866-2884.
23. Kappers, I.F., Aharoni, A., van Herpen, T., Luckerhoff, L.L.P., Dicke, M. and Bouwmeester, H.J. (2005) Genetic engineering of terpenoid metabolism attracts, bodyguards to Arabidopsis. Science 309 (5743), 2070-2072.
24. Dong, L., Jongedijk, E., Bouwmeester, H. and Van Der Krol, A. (2016) Monoterpene biosynthesis potential of plant subcellular compartments. New Phytologist 209 (2), 679-690.
25. Juneidi, S., Ting, H.M. and van der Krol, A. (2014) Tissue specific expression of a terpene synthase in *Nicotiana benthamiana* leaves. American Journal of Plant Sciences 5 (18), 2799.
26. Cunillera, N., Arró, M., Delourme, D., Karst, F., Boronat, A. and Ferrer, A. (1996) *Arabidopsis thaliana* contains two differentially expressed farnesyl-diphosphate synthase genes. Journal of Biological Chemistry 271 (13), 7774-7780.
27. Cunillera, N., Boronat, A. and Ferrer, A. (1997) The *Arabidopsis thaliana* FPS1 gene generates a novel mRNA that encodes a mitochondrial farnesyl-diphosphate synthase isoform. J Biol Chem 272 (24), 15381-15388.
28. Closa, M., Vranová, E., Bortolotti, C., Bigler, L., Arró, M., Ferrer, A. and Gruissem, W. (2010) The Arabidopsis thaliana FPP synthase isozymes have overlapping and specific functions in isoprenoid biosynthesis, and complete loss of FPP synthase activity causes early developmental arrest. The Plant Journal 63 (3), 512-525.
29. Manzano, D., Busquets, A., Closa, M., Hoyerova, K., Schaller, H., Kaminek, M., Arro, M. and Ferrer, A. (2006) Overexpression of farnesyl diphosphate synthase in Arabidopsis mitochondria triggers light-dependent lesion formation and alters cytokinin homeostasis. Plant Mol Biol 61 (1-2), 195-213.
30. Masferrer, A., Arró, M., Manzano, D., Schaller, H., Fernández-Busquets, X., Moncaleán, P., Fernández, B., Cunillera, N., Boronat, A. and Ferrer, A. (2002) Overexpression of Arabidopsis thaliana farnesyl diphosphate synthase (FPS1S) in transgenic Arabidopsis induces a cell death/senescence-like response and reduced cytokinin levels. Plant Journal 30 (2), 123-132.

819 31. Houshyani, B., Assareh, M., Busquets, A., Ferrer, A., Bouwmeester, H.J. and Kappers, I.F.
820 (2013) Three-step pathway engineering results in more incidence rate and higher emission of
821 nerolidol and improved attraction of Diadegma semiclausum. Metabolic Engineering 15 (0), 88-
822 97.
823 32. Dubin, M.J., Bowler, C. and Benvenuto, G. (2008) A modified Gateway cloning strategy for
824 overexpressing tagged proteins in plants. Plant Methods 4 (1), 3.
825 33. Curtis, M.D. and Grossniklaus, U. (2003) A Gateway cloning vector set for high-throughput
826 functional analysis of genes *in planta*. Plant Physiology 133 (2), 462-469.
827 34. Bevis, B.J. and Glick, B.S. (2002) Rapidly maturing variants of the Discosoma red
828 fluorescent protein (DsRed). Nat Biotech 20 (1), 83-87.
829 35. Liu, D.S., Shi, L.D., Han, C.G., Yu, J.L., Li, D.W. and Zhang, Y.L. (2012) Validation of
830 reference genes for gene expression studies in virus-infected *Nicotiana benthamiana* using
831 quantitative real-time PCR. Plos One 7 (9).
832 36. Pfaffl, M.W. (2001) A new mathematical model for relative quantification in real-time PCR.
833 Nucleic Acids Res 29 (9), 2002-2007.
834 37. Keim, V., Manzano, D., Fernández, F.J., Closa, M., Andrade, P., Caudepón, D., Bortolotti,
835 C., Vega, M.C., Arró, M. and Ferrer, A. (2012) Characterization of Arabidopsis FPS isozymes
836 and FPS gene expression analysis provide insight into the biosynthesis of isoprenoid precursors
837 in seeds. PLOS ONE 7 (11), e49109.
838 38. Vickers, C.E., Bongers, M., Liu, Q., Delatte, T. and Bouwmeester, H. (2014) Metabolic
839 engineering of volatile isoprenoids in plants and microbes. Plant, Cell & Environment 37 (8),
840 1753-1775.
841 39. Lange, B.M. and Ahkami, A. (2013) Metabolic engineering of plant monoterpenes,
842 sesquiterpenes and diterpenes—current status and future opportunities. Plant Biotech J 11 (2),
843 169-196.
844 40. Voinnet, O., Vain, P., Angell, S. and Baulcombe, D.C. (1998) Systemic spread of sequence-
845 specific transgene rna degradation in plants is initiated by localized introduction of ectopic
846 promoterless DNA. Cell 95 (2), 177-187.
847 41. Leuzinger, K., Dent, M., Hurtado, J., Stahnke, J., Lai, H., Zhou, X. and Chen, Q. (2013)
848 Efficient Agroinfiltration of Plants for High-level Transient Expression of Recombinant Proteins.
849 J Vis Exp (77), e50521.
850 42. van Herpen, T.W., Cankar, K., Nogueira, M., Bosch, D., Bouwmeester, H.J. and Beekwilder,
851 J. (2010) Nicotiana benthamiana as a production platform for artemisinin precursors. PLoS One
852 5 (12), e14222.
853 43. Brückner, K. and Tissier, A. (2013) High-level diterpene production by transient expression
854 in Nicotiana benthamiana. Plant Methods 9 (1), 46.
855 44. Tian, L. and Dixon, R.A. (2006) Engineering isoflavone metabolism with an artificial
856 bifunctional enzyme. Planta 224 (3), 496-507.
857 45. Juneidi, S., Ting, H.M. and van der Krol, A. (2014) Tissue specific expression of a terpene
858 synthase in *Nicotiana benthamiana* leaves. American Journal of Plant Sciences 2014.
859 46. Busquets, A., Keim, V., Closa, M., del Arco, A., Boronat, A., Arró, M. and Ferrer, A. (2008)
860 Arabidopsis thaliana contains a single gene encoding squalene synthase. Plant Molecular
861 Biology 67 (1), 25-36.
862 47. Leivar, P., Gonzalez, V.M., Castel, S., Trelease, R.N., Lopez-Iglesias, C., Arro, M., Boronat,
863 A., Campos, N., Ferrer, A. and Fernandez-Busquets, X. (2005) Subcellular localization of
864 Arabidopsis 3-hydroxy-3-methylglutaryl-coenzyme A reductase. Plant Phys 137 (1), 57-69.

48. Tholl, D., Boland, W., Hansel, A., Loreto, F., Röse, U.S. and Schnitzler, J.P. (2006) Practical approaches to plant volatile analysis. The Plant Journal 45 (4), 540-560.
49. Qualley, A.V. and Dudareva, N. (2014) Quantification of plant volatiles. In Plant Metabolism: Methods and Protocols (Sriram, G. ed), pp. 41-53.
50. Paula Barros, E., Moreira, N., Elias Pereira, G., Leite, S.G.F., Moraes Rezende, C. and Guedes de Pinho, P. (2012) Development and validation of automatic HS-SPME with a gas chromatography-ion trap/mass spectrometry method for analysis of volatiles in wines. Talanta 101, 177-186.
51. Wang, L.-F., Lee, J.-Y., Chung, J.-O., Baik, J.-H., So, S. and Park, S.-K. (2008) Discrimination of teas with different degrees of fermentation by SPME–GC analysis of the characteristic volatile flavour compounds. Food Chemistry 109 (1), 196-206.
52. Peña-Alvarez, A., Capella, S., Juárez, R. and Labastida, C. (2006) Determination of terpenes in tequila by solid phase microextraction-gas chromatography–mass spectrometry. Journal of Chromatography A 1134 (1–2), 291-297.
53. Williams, A., Ryan, D., Olarte Guasca, A., Marriott, P. and Pang, E. (2005) Analysis of strawberry volatiles using comprehensive two-dimensional gas chromatography with headspace solid-phase microextraction. Journal of Chromatography B 817 (1), 97-107.
54. Aharoni, A., Jongsma, M., Kim, T.-Y., Ri, M.-B., Giri, A., Verstappen, F.A., Schwab, W. and Bouwmeester, H. (2006) Metabolic engineering of terpenoid biosynthesis in plants. Phytochemistry Reviews 5 (1), 49-58.
55. Yang, T., Stoopen, G., Yalpani, N., Vervoort, J., de Vos, R., Voster, A., Verstappen, F.W.A., Bouwmeester, H.J. and Jongsma, M.A. (2011) Metabolic engineering of geranic acid in maize to achieve fungal resistance is compromised by novel glycosylation patterns. Metabolic Engineering 13 (4), 414-425.

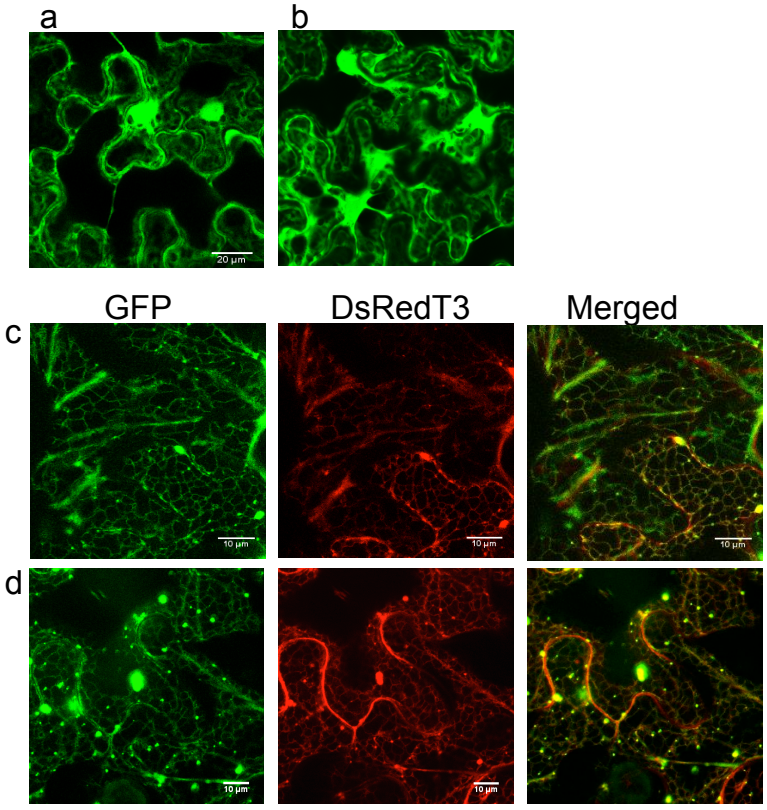

Figure 1. Confocal micrographs of tobacco epidermal parenchyma 3 days after agroinfiltration with *Agrobacterium tumefaciens* harboring a binary plasmid for the expression of GFP alone (a), FaNES1 fused to GFP (b), or FaNES1 fused to the transmembrane domain of HMGR1S (c) or SQS (d). The GFP signals of (c) and (d) correspond to a reticulate structure which co-localizes with the signal for DsRedT3, a marker for the ER membrane (merged signals shown at right). The GFP control, in contrast, is dispersed throughout the cell and is typical of soluble expression in the cytosol. Bar = 20 μm (a and b) or 10 μm (c and d).

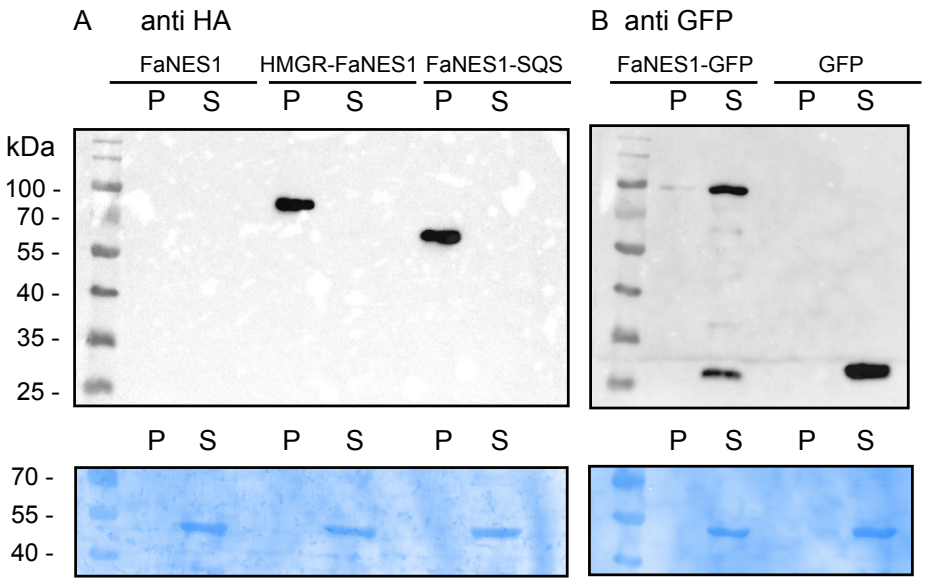

Figure 2. Western blot analysis using anti-HA (A) and anti-GFP (B) antibodies of microsomal (P) and soluble (S) cell fractions from leaves expressing the recombinant FaNES1 proteins and GFP. The predicted molecular weight of FaNES1 proteins is approximately 50.0 kDa (FaNES1-3HA), 83.6 kDa (HMGR-FaNES1-3HA), 71.3 kDa (3HA-FaNES1-SQS), 87.3 kDa (FaNES1-GFP). Coomassie Brilliant Blue-stained large subunit of Rubisco in blotted membranes is shown at the bottom. The position of protein molecular-weight standards is shown on the left.

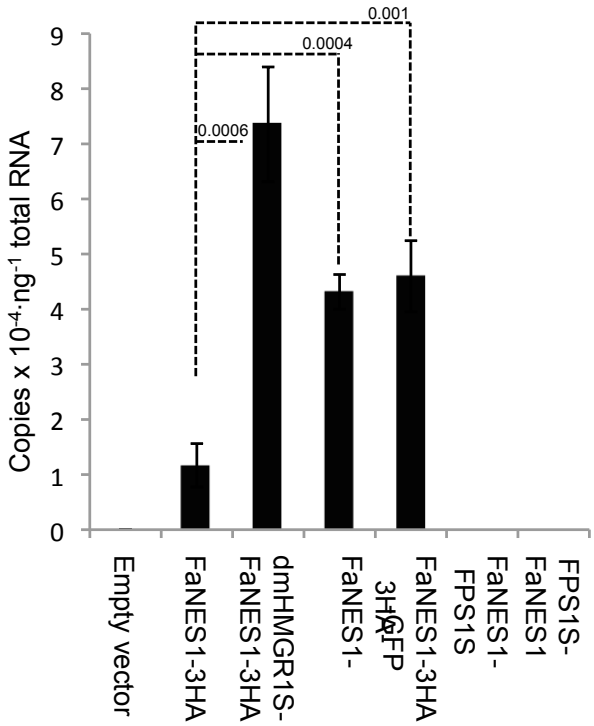

Figure 3. Absolute transcript abundance of FaNES1 detected in agroinfiltrated *N. benthamiana*. cDNA loading was normalized using the Ct value of reference gene *PP2A*, and the corrected signal was compared to a standard curve constructed from serial dilutions of a purified plasmid containing FaNES1. Values shown represent the average of 3 biological replicates (n = 3). Error bars signify the standard deviation. 3HA indicates three tandem copies of the hemagglutinin epitope used for Western blot detection. p values for a two tailed t-test are displayed for the corresponding comparison to FaNES1-3HA.

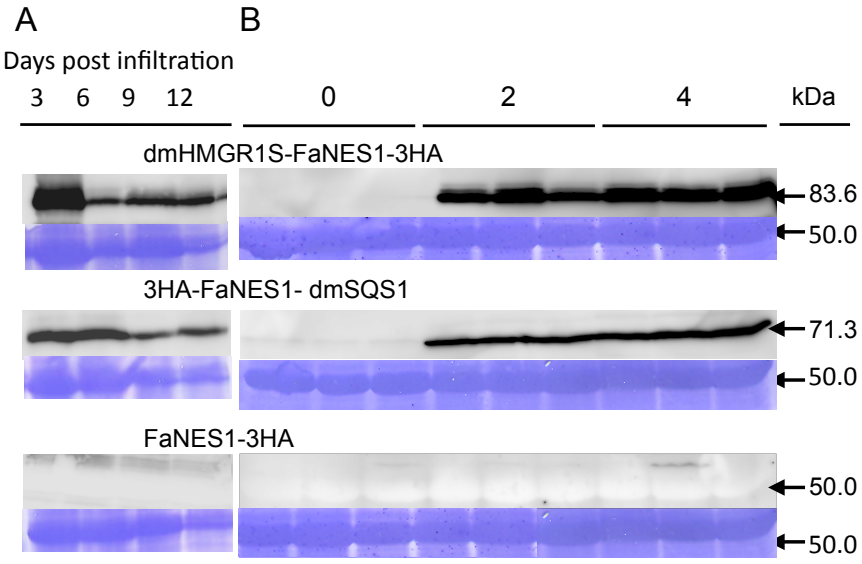

Figure 4. Western blot showing an extended (A) or short term (B) time course of protein accumulation in agroinfiltrated *N. benthamiana* leaf tissue from 0-12 days post infiltration (dpi). The accumulation of FaNES1 fused to the transmembrane domain of HMGR1S at its N-terminus (dmHMGR1S-FaNES1-3HA), the transmembrane domain of SQS1 at its C-terminus (3HA-FaNES1-dmSQS1), or soluble FaNES (FaNES-3HA) are shown. All proteins contained a triple HA epitope for antibody detection. Uniform protein loading of the gel was verified by Coomassie blue staining of Rubisco large subunit (bottom).

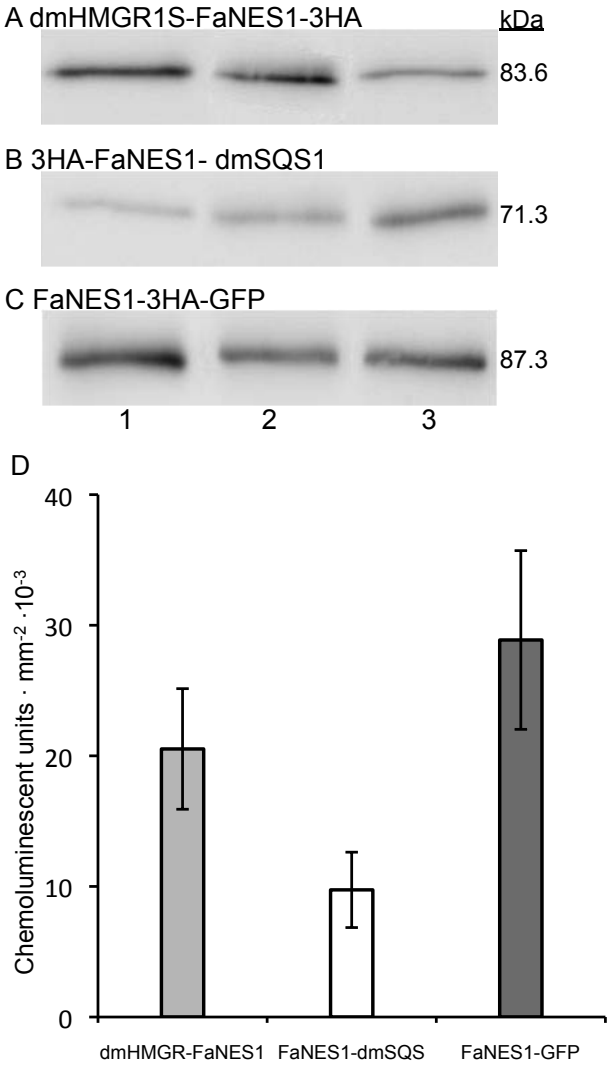

Figure 5. Chemoluminescence imaging of a Western blot showing relative expression levels of three FaNES1 constructs targeted to the ER (A and B) or fused to GFP as a soluble protein (C). Agroinfiltrated tobacco leaves transfected with one of the three constructs shown above were harvested 2 days post infiltration. A 2.5 μg aliquot of total protein was electrophoresed on a 9% SDS-PAGE gel, transferred to a PVDF membrane, and imaged via bioluminescent assay of the resulting Western blot, as described in methods. Three independent replicates are shown for each construct. The FaNES1-GFP fusion showed consistently higher protein accumulation levels. D, chemoluminescent signal intensity of the band corresponding to each transgene product shown in A-C (n = 3, error bars represent the standard error).

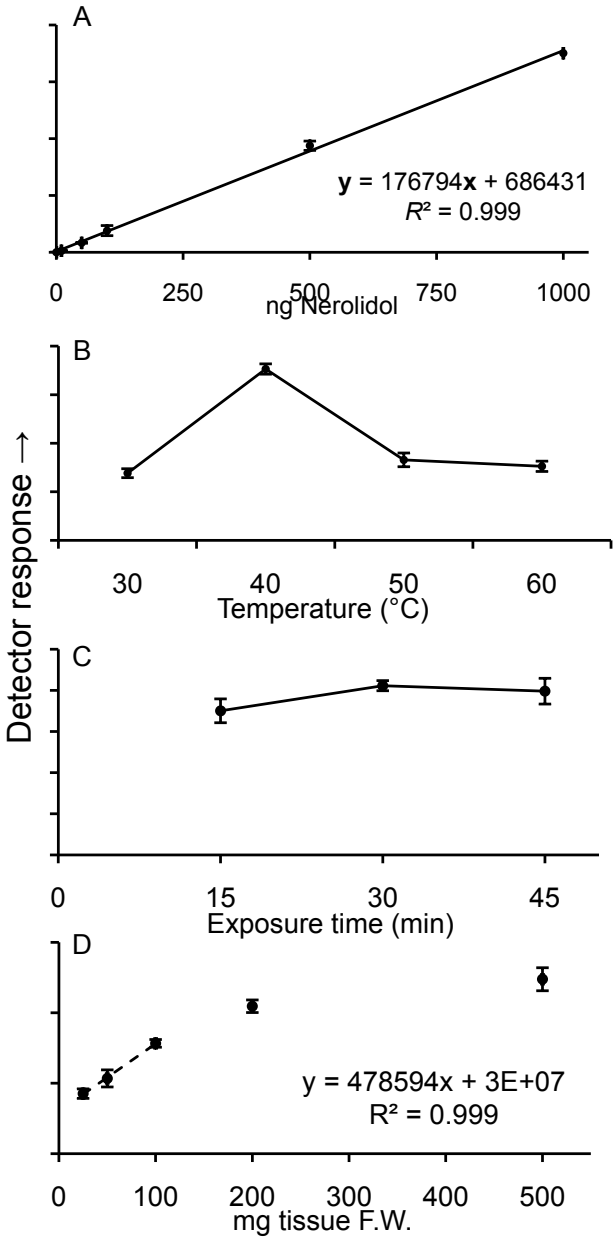

Figure 6. Optimization of nerolidol quantification by SPME-GCMS. A, differing amounts of nerolidol were added to a headspace vial to determine the linear range of the detector response. Over the likely range of nerolidol production in tobacco, the response range was linear. B, SPME fiber incubations with nerolidol standard were carried out at different temperatures to determine the optimal binding temperature. C, Exposure times ranging from 15 min – 45 min were assays to assess the optimal incubation time. D, Nerolidol standard was assayed in the presence of variable amounts of fresh ground tobacco tissue ranging from 10 mg – 500 mg to assess matrix effects. Beyond 100 mg tissue, significant matrix effects were evident.

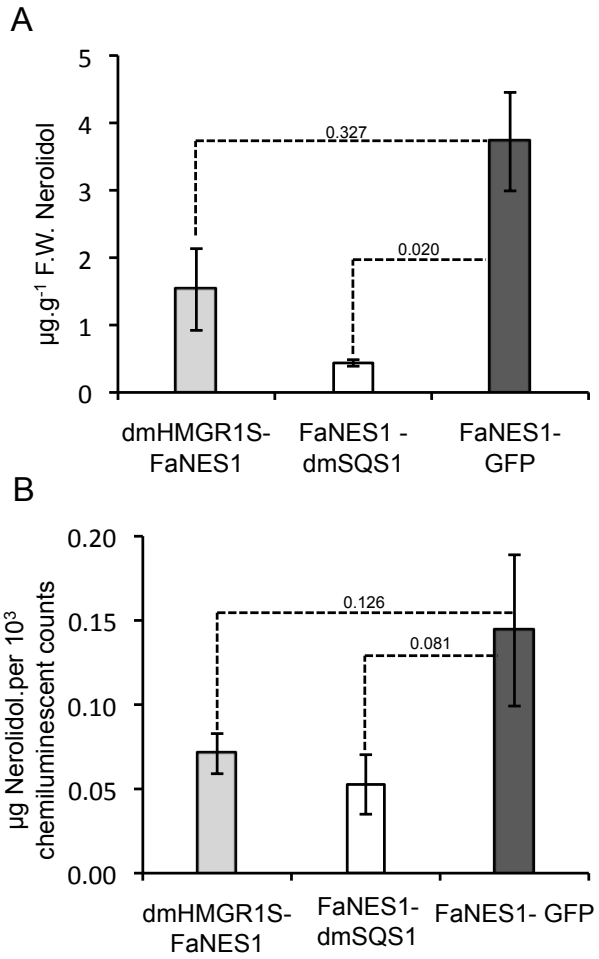

Figure 7. Nerolidol production in agroinfiltrated tobacco leaves normalized to tissue fresh weight (A) or FaNES1 protein accumulation level (B). Three biological replicates were analyzed per group. Values shown are uncorrected but internal standard recoveries were typically 3-4%. Actual nerolidol production may therefore be much higher.

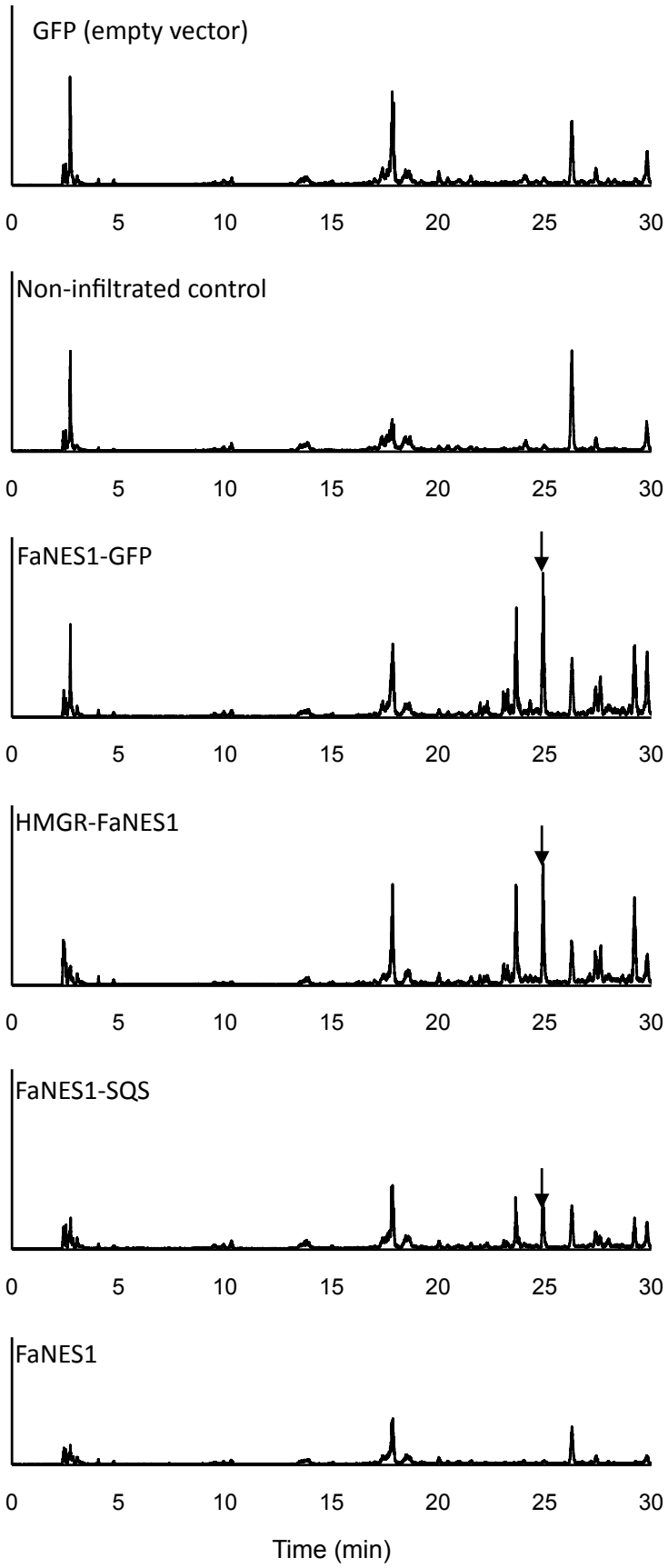

Figure 8. LCMS/MS analysis of methanolic extracts of agroinfiltrated tobacco leaf tissue. Q_1 multiple ion monitoring was performed in positive mode to survey nearly a dozen conjugated forms of nerolidol ranging in mass from *m/z* 456 to 690. Peaks also detected in empty vector infiltration controls were ruled out from this comparison. Three individual tobacco plants were infiltrated with each construct. A single representative chromatogram is shown for each construct. The arrow represents one of several nerolidol conjugates used to infer the accumulation of non-volatile forms of nerolidol which was absent from controls. This peak (24.92) matches the expected mass of hydroxynerolidol-malonyl-ketopentoside (457.2 [$M+H^+$]) (Houshyani et al. 2013).

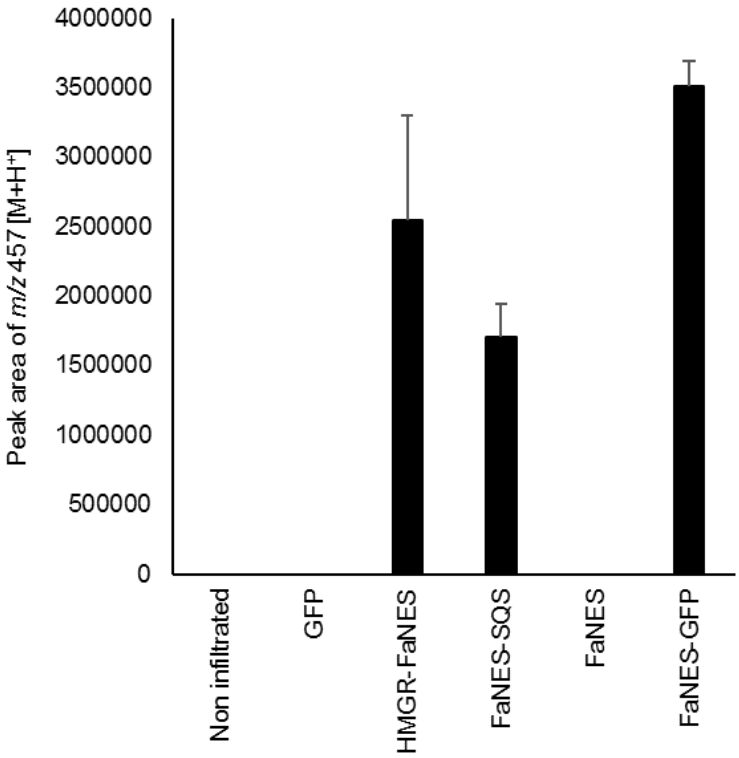

Figure 9. Relative quantification of a non-volatile nerolidol conjugate in agroinfiltrated tobacco leaves. A peak eluting at approximately 24.92 min representing hydroxynerolidol-malonyl-ketopentoside (Houshyani et al. 2013) was used to compare the accumulation of conjugated nerolidol glycosides. This peak was absent in non-infiltrated and empty vector controls and was used to infer accumulation of conjugated forms of nerolidol. Their accumulation closely mirrors the ratios of free nerolidol detected by GCMS in the same treatment groups. The data shown represent peak area normalized to sample mass. Error bars represent the standard error of 3 independent biological replicates.

Supplementary data
Andrade et al. (2017)

Figure 4A – complete gel image

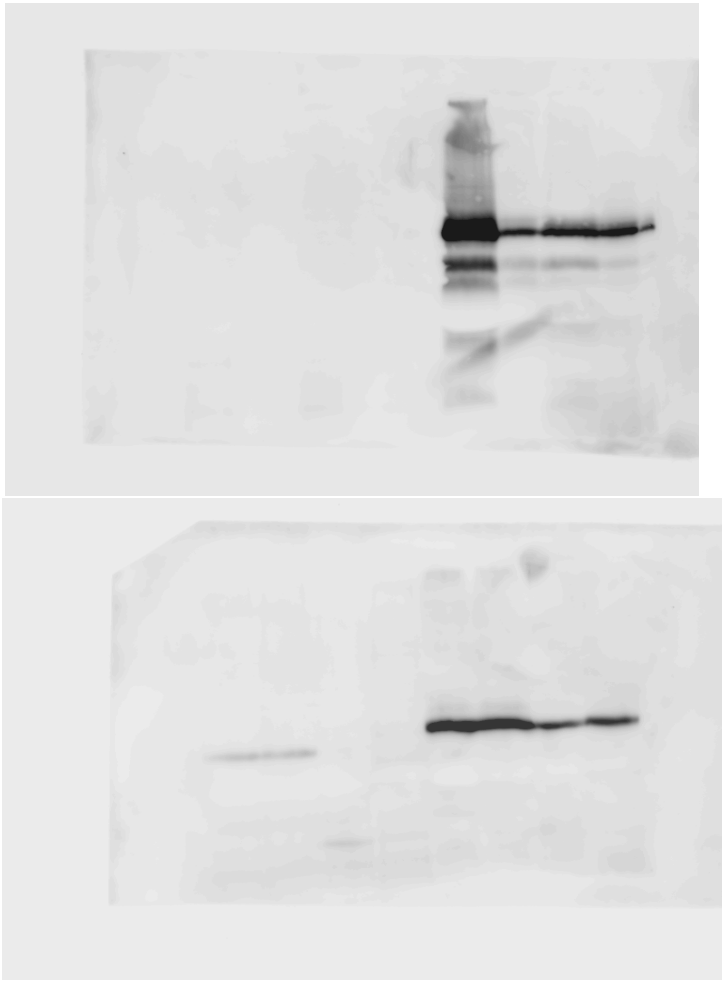

Supplementary data 2
Andrade et al. (2017)

Figure 4B – complete gel image